Long-Term Period Behavior of the Semiregular Variable V1 and the Type II Cepheids V2 and V3 in the Globular Cluster M10

Pradip Karmakar
Department of Mathematics, Madhyamgram High School (H.S.), Sodepur Road, Madhyamgram, Kolkata-700129, India; pradipkarmakar39@gmail.com

Horace A. Smith
Department of Physics and Astronomy, Michigan State University, East Lansing, MI 48824; smithhh@msu.edu

Wayne Osborn
Department of Physics, Central Michigan University, Mount Pleasant, MI 48859; wayne.osborn@cmich.edu

Peter B. Stetson
NRC-Herzberg, Dominion Astrophysical Observatory, 5071 West Saanich Road, Victoria BC V9E 2E7, Canada; Peter.Stetson@nrc.ca

Received January 7, 2022; revised March 28, 2022; accepted April 1, 2022

Abstract We present new U, B, V, R_C, and I_C-band photometry for the semiregular variable V1 and the type II Cepheids V2 and V3 in the globular cluster M10. Using old and new observations, we updated the most recent—1985—period change study of these variables. Observations made from 1912 through 2020 show that V1 has a recent average period of 48.9 days and, for the Cepheid variables, the 18.7-day pulsation period of V2 has decreased and the 7.8-day pulsation period of V3 has remained constant. The Fourier spectrum of the V-band observations of V2 yields a pattern of additional peaks at $0.5f_0$ and $1.5f_0$, where $f_0$is the frequency of the fundamental mode, similar to those that have been reported for W Virginis that indicate probable period-doubling.

1. Introduction

The period of a pulsating variable star is a basic parameter for determining its type (see Samus *et al.* 2017). Furthermore, periods of regularly pulsating stars can often be determined more accurately than any other of their measurable quantities, and observing changes in period have the potential to reveal evolution effects of a pulsating star before it shows in any other manner.

In this paper we study the light curves and period behavior of three variables in the globular cluster M10 (NGC 6254, C1654-040): V1, V2, and V3 (Table 1). A finding chart is given by Clement *et al.* (1985). One of these stars, V1, is a red semiregular variable. The other two, V2 and V3, are type II Cepheids with periods of 18.7 days and 7.8 days, respectively. Type II Cepheids of periods longer than about 5 days, such as V2 and V3, are classified as W Virginis type, while those with shorter periods are designated BL Herculis variables (Soszyński *et al.* 2011, Figure 4; Bono *et al.* 2020). Our study extends the period change analyses of these stars by Clement *et al.* (1985), and compares our results to other observed rates of period change for type II Cepheids.

Table 1. Coordinates from the *Catalogue of Variable Stars in Galactic Globular Clusters* (Clement *et al.* 2001).

Object	*R.A. (J2000)* h m s	*Dec. (J2000)* ° ‘ “
V1	16 57 10.12	–04 05 36.1
V2	16 57 11.74	–04 03 59.7
V3	16 56 55.95	–04 04 16.3

2. The observational data sets

We draw upon five sets of photometric observations of M10 that date from 1983, the date of the last observations included in the Clement *et al.* (1985) investigation: (1) the archival U, B,V, R_C, and I_C CCD photometry compiled by Stetson *et al.* (2019, hereafter referred to as “Stetson”); (2) B,V, and I_C CCD photometry from the Michigan State University Observatory (MSU); (3) V and R_C CCD photometry (for V1 only) from the National Undergraduate Research Observatory (NURO); (4) V-band and g-band data from the All-Sky Automated Survey for Supernovae (ASAS-SN); and (5) B and V brightness estimates on photographic plates from the United States Naval Observatory (USNO) and the Las Campanas and Hale Observatories.

Data Set 1 The Stetson photometry was obtained from heterogeneous archival CCD images from many observatories and observing runs, reduced and calibrated in a consistent way by one of the authors (PBS). His approach to this data reduction is described in Stetson *et al.* (2019). Observations of primary and secondary photometric standard fields obtained during each run were used to derive the color-transformation and extinction corrections for each night. These were used to transform instrumental magnitudes to the Landolt photometric system. The heterogeneous nature of the Stetson photometry is illustrated in Table 2, which shows the data from three of the 32 observing runs used: Run 7 and Run 9 with the La Silla ESO 2.2-m telescope in 2000 and 2001, Run 10 with the La Palma 1-m telescope in 2002. The complete photometry is included in the AAVSO ftp site[1] in a somewhat different format.

Table 2. A sample of the Stetson CCD U, B, V, R_C, and I_C photometry of V1, V2, and V3.

Run	*HJD*	*Filter*	*V1*	*Error*	*V2*	*Error*	*V3*	*Error*
7	2451633.8891	B	13.528	0.0040	13.065	0.0037	13.676	0.0051
7	2451633.8930	B	13.471	0.0110	13.057	0.0043	13.639	0.0077
7	2451633.8969	B	13.478	0.0113	13.048	0.0071	13.645	0.0054
7	2451635.9030	V	12.008	0.0045	12.453	0.0050	12.579	0.0053
7	2451635.9068	V	12.006	0.0041	12.453	0.0076	12.562	0.0054
7	2451635.9106	V	12.002	0.0049	12.455	0.0049	12.562	0.0071
7	2451635.8934	I_C	10.383	0.0080	11.108	0.0051	11.619	0.0050
7	2451635.8971	I_C	10.381	0.0141	11.120	0.0068	11.604	0.0046
7	2451635.9016	I_C	10.397	0.0159	11.111	0.0041	11.601	0.0052
9	2451998.8970	U	—	—	12.415	0.0043	13.922	0.0040
9	2451998.9030	U	14.465	0.0046	12.421	0.0043	13.922	0.0036
9	2451998.8730	B	—	—	12.104	0.0037	13.528	0.0041
9	2451998.8742	B	13.237	0.0054	12.087	0.0044	13.529	0.0046
9	2451998.8573	V	—	—	11.448	0.0038	12.700	0.0029
9	2451998.8586	V	11.772	0.0036	11.443	0.0027	12.705	0.0037
9	2451998.8637	V	—	—	11.476	0.0032	12.684	0.0017
9	2451998.8706	V	11.768	0.0051	11.464	0.0034	12.680	0.0026
9	2451998.8853	V	—	—	11.459	0.0038	12.684	0.0032
9	2451998.8899	V	11.773	0.0046	11.459	0.0039	12.687	0.0021
10	2452404.5846	B	13.684	0.0093	13.532	0.0055	—	—
10	2452404.5821	V	12.150	0.0198	12.584	0.0156	—	—
10	2452404.5791	R_C	11.356	0.0222	11.946	0.0118	—	—

The complete photometry is included in the AAVSO ftp site in a somewhat different format (ftp://ftp.aavso.org/public/datasets/501-Karmakar-StetsonPhotometry.txt). *A summary table of the Stetson photometry observing runs is also available there* (ftp://ftp.aavso.org/public/datasets/501-Karmakar-StetsonSummary.txt).

Data Set 2 We obtained B, V, and I_C-band images of M10 in 2006 using the 0.6-m telescope of the Michigan State University (MSU) campus observatory with an Apogee Alta U47 CCD camera (0.6 arc-second pixels, 10 × 10 arcmin field of view). Bias and dark images were subtracted in the conventional way and twilight images were used as flat field images. Exposures were about 1-minute long, varying somewhat with sky conditions. Instrumental photometry was obtained using the DAOPHOT and ALLSTAR routines (Stetson 1987, 1994), as in Rabidoux *et al.* (2010). Standard stars for calibration of instrumental photometry to the standard B, V, and I_C systems were selected from the photometry in Stetson's web-based catalogue[2] (Stetson *et al.* 2019, Table 4). Six to ten relatively unblended stars were used to set the zero-point for each filter. Color terms were applied as in Rabidoux *et al.* (2010). The MSU photometry obtained in this way produces light curves that closely match those from the Stetson photometry. The MSU observations are listed in Table 3.

Data Set 3 We located archival V and R_C CCD images of M10 obtained over four consecutive nights in 2004 from the 0.8-m telescope of the National Undergraduate Research Observatory (NURO). The small 4 × 4 arcmin field of view meant that only V1 was visible on these images. They were reduced in a similar manner as for the MSU observations. The resulting magnitudes are given in Table 4.

Data Set 4 We downloaded observations of V1, V2, and V3 from the All-Sky Automated Survey for Supernovae (ASAS-SN; Shappee *et al.* 2014; Kochanek *et al.* 2017) from the Sky Patrol option on the ASAS-SN webpage, using the positions for the variables given in Table 1. Only V-band observations are available for most of the 2012–2020 time period we utilized, although g-band data are more recently available, including for 2020. The different cameras used to collect the ASAS-SN data sometimes have slightly different zero-points, resulting in increased light curve scatter. In the cases of the M10 observations, these shifts, if present, appear to be smaller than a few hundredths of a magnitude and we have not applied corrections for them. The relatively large ASAS-SN pixels mean, however, that these observations show the effects of blending more seriously than is the case for the MSU and Stetson CCD photometry. This is somewhat mitigated for V2 and V3 because they are not close to the center of the cluster.

Data Set 5 Finally, we made use of archival photographic plates. We possessed 20 plates (ten B and ten V plates) of M10 taken with the USNO-Flagstaff, Arizona, 1.5-m reflector over a 24-day span in 1983. To these we added six Las Campanas plates taken 1992–1993 and one Hale (Mt. Wilson) plate from 1932 found in the Yerkes Observatory plate vault. All but the Hale plate were exposed with filter and emulsion combinations that gave images approximating either B or V magnitudes. Magnitudes for the variable stars were derived by eye estimates of the variable's brightness relative to several non-variable stars having Stetson *et al.* (2019) photometry. Because V1, V2, and V3 are among the very brightest stars in the cluster, there are only a few suitable comparison stars and at times magnitude estimates had to be made by extrapolating from the comparison sequence, leading to significant uncertainties.

Five to ten independent brightness estimates were made for each plate using a loupe. The average of the different estimates for a star yielded its adopted magnitude while their dispersion

[1] ftp://ftp.aavso.org/public/datasets/501-Karmakar-StetsonPhotometry.txt
[1] https://www.canfar.net/storage/vault/list/STETSON/homogeneous/Latest_photometry_for_targets_with_at_least_BVI/NGC6254_(UBVRI)

Table 3. The MSU CCD photometry of V1, V2, and V3.

HJD	*Filter*	*V1*	*Error*	*V2*	*Error*	*V3*	*Error*
2453892.6279	B	13.11	0.02	12.25	0.02	13.32	0.02
2453895.6290	B	13.18	0.02	12.58	0.02	13.75	0.02
2453899.6211	B	13.18	0.03	13.46	0.02	13.37	0.02
2453901.6280	B	13.20	0.03	13.40	0.02	13.44	0.02
2453903.6192	B	13.31	0.03	13.08	0.02	13.75	0.02
2453906.6196	B	13.22	0.02	11.97	0.02	13.50	0.02
2453907.6175	B	13.27	0.03	12.09	0.02	13.26	0.02
2453907.6200	B	13.30	0.03	12.11	0.02	13.26	0.02
2453935.6317	B	13.33	0.03	13.21	0.02	13.67	0.02
2453936.6353	B	13.35	0.03	13.35	0.02	13.59	0.02
2453937.6154	B	13.29	0.03	13.49	0.02	13.43	0.02
2453943.6025	B	13.19	0.03	12.01	0.02	13.77	0.02
2453892.6230	V	11.88	0.03	11.45	0.02	12.60	0.02
2453895.6252	V	12.00	0.03	11.69	0.02	12.92	0.02
2453899.6179	V	11.99	0.03	12.43	0.02	12.52	0.02
2453901.6259	V	12.13	0.03	12.46	0.02	12.58	0.02
2453903.6175	V	12.17	0.03	12.39	0.02	12.90	0.02
2453906.6172	V	12.06	0.03	11.53	0.02	12.69	0.02
2453907.6159	V	12.10	0.03	11.48	0.02	12.54	0.02
2453910.6284	V	—	—	11.47	0.02	12.75	0.02
2453910.6314	V	12.10	0.04	11.49	0.02	12.78	0.02
2453935.6341	V	12.13	0.03	12.52	0.02	13.02	0.02
2453936.6375	V	12.16	0.02	12.38	0.02	12.86	0.02
2453937.6205	V	12.18	0.03	12.40	0.02	12.64	0.02
2453943.6050	V	12.01	0.03	11.45	0.02	12.98	0.02
2453892.6303	I_C	10.32	0.02	10.52	0.02	11.60	0.02
2453892.6317	I_C	10.36	0.02	10.55	0.02	11.62	0.02
2453895.6326	I_C	10.40	0.03	10.60	0.02	11.91	0.02
2453899.6254	I_C	10.37	0.03	11.37	0.02	11.63	0.02
2453901.6301	I_C	10.40	0.03	11.34	0.02	11.58	0.02
2453903.6242	I_C	10.43	0.03	11.29	0.02	11.88	0.02
2453935.6279	I_C	10.34	0.03	11.19	0.02	11.97	0.02
2453906.6220	I_C	10.38	0.03	10.65	0.02	11.70	0.02
2453907.6218	I_C	10.39	0.03	10.57	0.02	11.56	0.02
2453910.6207	I_C	10.42	0.03	10.51	0.02	11.72	0.02
2453936.6333	I_C	10.46	0.02	11.24	0.02	11.72	0.02
2453936.6344	I_C	10.41	0.03	11.28	0.02	11.80	0.02
2453937.6180	I_C	10.30	0.03	11.31	0.02	11.66	0.02
2453937.6195	I_C	10.35	0.03	11.35	0.02	11.67	0.02
2453943.6001	I_C	10.32	0.03	10.70	0.02	11.90	0.02

Table 4. The NURO CCD V and R_C photometry of V1.

HJD	*Filter*	*Mag.*	*Error*
2453140.7692	V	12.007	0.038
2453140.7697	V	12.016	0.023
2453140.7704	V	11.979	0.016
2453141.9262	V	11.944	0.015
2453141.9270	V	11.929	0.020
2453142.8997	V	11.923	0.018
2453142.9006	V	11.908	0.031
2453143.8416	V	11.899	0.009
2453143.8424	V	11.895	0.020
2453140.7669	R_C	11.115	0.028
2453140.7674	R_C	11.124	0.013
2453140.7681	R_C	11.134	0.017
2453141.9283	R_C	11.078	0.016
2453141.9289	R_C	11.090	0.013
2453142.9016	R_C	11.083	0.008
2453142.9023	R_C	11.097	0.015
2453143.8434	R_C	11.061	0.026
2453143.8442	R_C	11.061	0.024

indicated the error. Including possible magnitude zero-point errors, we adopt as the uncertainties in our photographic magnitudes: 0.20 mag for V1, 0.15 mag for V2, and 0.10 mag for V3 from the USNO B and V plates, 0.12 mag from the Las Campanas B and V plates, and 0.10 mag from the Hale B plate. The photographic data are given in Table 5.

3. Periods and light curves

We used two period-finding routines to search for periodicities in the V1, V2, and V3 data: Period04 (Lenz and Breger 2005) and a date-compensated discrete Fourier transform, as implemented in Peranso 2.0 (Vanmunster 2006; Paunzen and Vanmunster 2016). Independent searches were carried out on the combined MSU and Stetson B, V, and I_C photometry and on the ASAS-SN photometry. No single period was found that produced a good phased light curve for V1 for all the MSU-Stetson data. This is probably a consequence of the semiregular nature of the variations and the relatively large number of years (1996–2018) spanned by those observations.

Table 5. B and V magnitudes from USNO, Las Campanas (LC) and Hale photographic plates for V1, V2, and V3.

Plate Number	*Filter*	*HJD*	*V1*	*V2*	*V3*
USNO 48325	B	2445496.7880	13.09	13.57	13.44
USNO 48327	B	2445496.7949	13.07	13.62	13.45
USNO 48486	B	2445514.7727	13.42	13.51	13.57
USNO 48488	B	2445514.7803	13.46	13.57	13.54
USNO 48516	B	2445516.7472	13.44	13.73	13.94
USNO 48518	B	2445516.7542	13.45	13.72	13.79
USNO 48556	B	2445519.7549	13.42	13.65	13.50
USNO 48558	B	2445519.7628	13.39	13.72	13.55
USNO 48579	B	2445520.7827	14.36	13.60	13.54
USNO 48581	B	2445520.7897	13.43	13.62	13.49
LC CD-2964	B	2448800.674	—	12.40	13.38
LC CD-2965	B	2448800.684	—	12.57	13.40
LC CD-2966	B	2448800.695	—	12.36	13.41
LC CD-2967	B	2448800.707	—	12.48	13.41
Hale B61	B	2426799.978	—	12.57	13.95
USNO 48324	V	2445496.7852	11.90	12.14	12.75
USNO 48326	V	2445496.7915	11.89	12.18	12.80
USNO 48485	V	2445514.7688	12.04	12.03	12.75
USNO 48487	V	2445514.7765	11.97	11.93	12.83
USNO 48517	V	2445516.7511	12.10	12.60	13.05
USNO 48519	V	2445516.7574	12.08	12.53	13.03
USNO 48557	V	2445519.7588	12.08	12.58	12.85
USNO 48559	V	2445519.7668	12.07	12.57	12.80
USNO 48578	V	2445520.7791	12.09	12.54	12.78
USNO 48580	V	2445520.7862	12.03	12.51	12.83
LC CD-3043	V	2449158.641	—	11.50	12.98
LC CD-3044	V	2449158.651	—	11.65	12.94

Table 6. Period search results for V1, V2, and V3 data with Period04 and the Peranso 2.0 DCDFT routine.

Data Set	*Period04 Result (d)*	*Peranso 2.0 Result (d)*
V1-ASAS-SN g-data	48.94 ± 0.10	48.95 ± 0.25
V1-ASAS-SN V-data	48.89 ± 0.02	48.90 ± 0.10
V2-ASAS-SN g-data	18.70 ± 0.02	18.70 ± 0.06
V2-Stetson & MSU B-data	18.703 ± 0.005	18.702 ± 0.010
V2-ASAS-SN V-data	18.702 ± 0.005	18.701 ± 0.008
V2-Stetson & MSU V-data	18.704 ± 0.005	18.707 ± 0.010
V2-Stetson & MSU I_C-data	18.70 ± 0.02	18.71 ± 0.01
V3-ASAS-SN g-data	7.833 ± 0.002	7.833 ± 0.003
V3-Stetson & MSU B-data	7.8330 ± 0.0004	7.8331 ± 0.0008
V3-ASAS-SN V-data	7.8343 ± 0.0005	7.8351 ± 0.0008
V3-Stetson & MSU V-data	7.8329 ± 0.0006	7.8330 ± 0.0009
V3-Stetson & MSU I_C-data	7.834 ± 0.001	7.833 ± 0.002

Table 7. Frequency and Amplitude results of V2 in V band.

Frequence (c/d)	*Amplitude V*	*ID*
0.0534849(11)	0.439(2)	f_0
0.1069698	0.099(2)	$2f_0$
0.1604547	0.059(2)	$3f_0$
0.213940	0.045(2)	$4f_0$
0.267424	0.022(2)	$5f_0$
0.320909	0.009(2)	$6f_0$
0.026676(12)	0.042(2)	$f_{(low)}$
0.080222(13)	0.038(2)	f_1

On the other hand, consistent periods were found in more numerous ASAS-SN V and g-band observations of 2012–2020. We found unique periods for V2 and V3 that fit the Stetson-MSU and ASAS-SN data. The period search results are given in Table 6, which shows that the Period04 and Peranso results agree well. For Period04, the listed uncertainties derive from the least squares fitting routine, while for the Peranso 2.0 results, uncertainties depend upon the noise in the amplitude spectrum, which we estimated independently of the default values in the Peranso routine.

Variable 1 Figure 1 shows the U, B, V, R_C, and I_C-band light curves for V1 from our CCD data, i.e. from the Stetson, MSU, and NURO sources. Brightness changes over 0.5 mag are seen. Figure 2 shows the light curve for just one observing season, 2018, using the ASAS-SN data. Cycle-to-cycle variations are clearly seen, as is often the case for red giant variables. Other observing seasons show similar effects. Finally, Figure 3 shows that the ASAS-SN data yield a reasonable phased light curve assuming an average period of 48.9 days since 2012. This agrees with the "a little less than 50 days" period found by Clement *et al.* (1985), but is significantly shorter than the period of 70.88 published by Rozyczka *et al.* (2018).

Variable 2 The phased U, B, V, R_C, and I_C light curves of V2 using a period of 18.703 days from the Stetson (dots) and MSU (Xs) CCD photometry are shown in Figure 4. Figure 5 and Figure 6 present the light curves using the same reference epoch and period for the ASAS-SN V observations and the photographic data, respectively. The phase shifts of the photographic light curves compared to the CCD ones in Figures 4 and 5 likely reflect the changing period as discussed in the following section.

The Figure 4 light curves show broad maxima and that the times (i.e., phase) of maximum and of minimum light increase somewhat with longer wavelength; these effects were noted by Arp (1955). The detailed nature of the broad maximum—called double-peaked by Arp—is obvious in the ASAS-SN data of Figure 5, but those observations average about 0.3 mag brighter than ours. We note that our period supports the 18.7226-day period for V2 found by Clement *et al.* (1985) but disagrees with the 19.470995-day period found by Rozyczka *et al.* (2018). We suspect this is due to an incorrect cycle count being used in linking their 1998 and 2002 observation sets.

Arp (1955) suggested that the amplitude of the light curve of V2 might differ in alternate cycles of the 18.7-day period. This effect (commonly called period doubling), was discovered in RV Tauri variables—Cepheid-like pulsating stars with periods longer than 20 days—but now has been seen in the two type II Cepheid subtypes, the BL Her and W Vir stars (for more details see Smolec and Moskalik 2012, Plachy *et al.* 2017, Smolec *et al.* 2018 and references therein). Period doubling in V2 is seen in our observations, most clearly in the numerous ASAS-SN V data. Figure 7 presents the ASAS-SN light curve of V2 phased with a 37.406-day period, twice our adopted P = 18.703 days. Although one could regard V2 as having a true period of 37.4 days, we retain the 18.7-day period in studying its long term period changes. As noted by Clement *et al.* (1985), the early photographic observations are not adequate for using the doubled period.

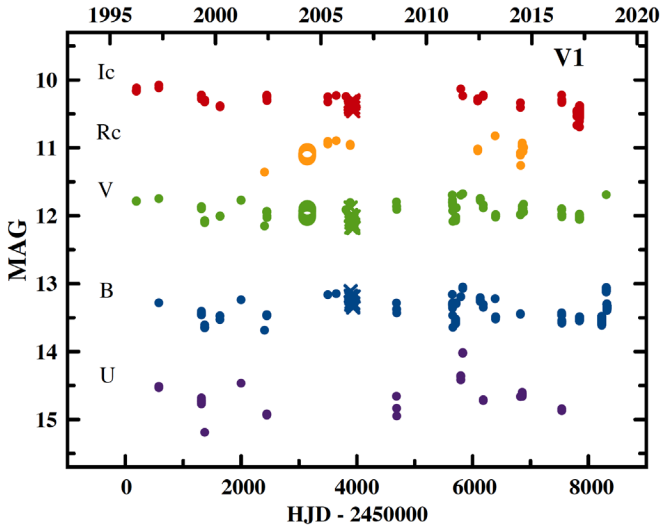

Figure 1. The U, B, V, R_C, and I_C-band light curves of V1 from 1996 to 2018 from our CCD data (Data sets 1–3). Observations from Stetson are shown as dots, those from MSU as Xs, and those from NURO as open circles.

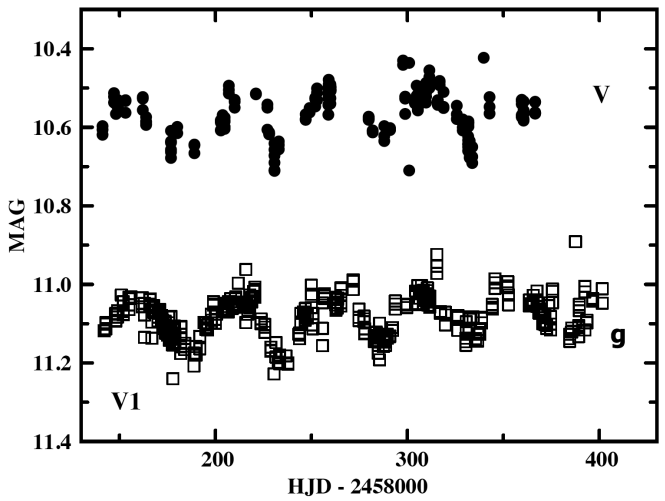

Figure 2. Light curves of V1 from the ASAS-SN V-band and g-band observations for the 2018 observing season. V data are represented by closed circles and g-data by open squares. The semiregular nature of the variations on a time scale of about 50 days is seen in the figure.

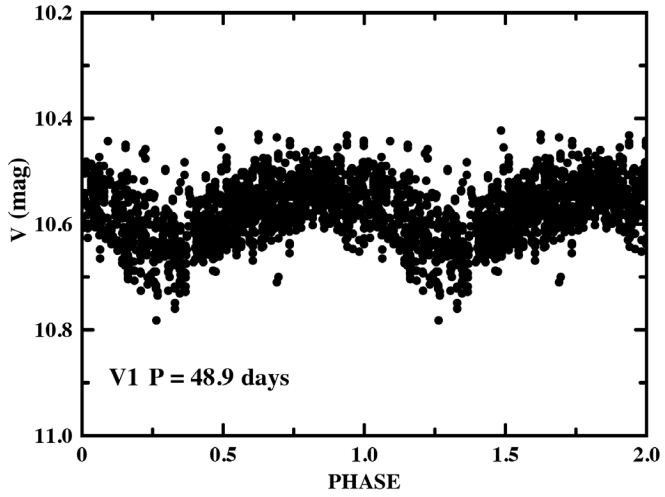

Figure 3. The phased light curve of V1 from all ASAS-SN V-band observations using a period of 48.9 days.

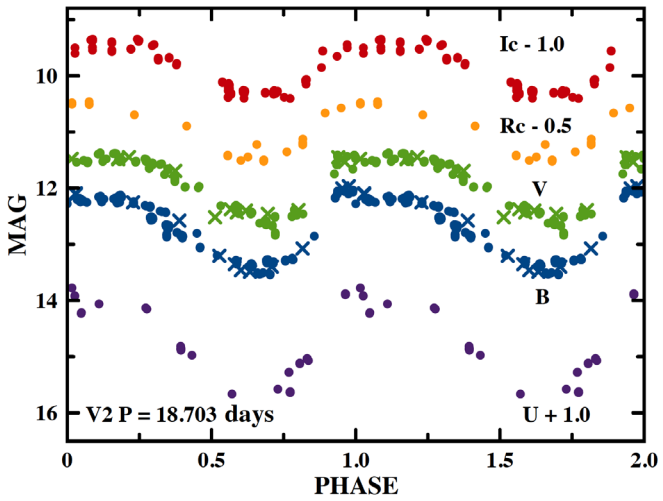

Figure 4. The U, B, V, R_C, and I_C-band phased light curves of V2 from the Stetson (dots) and MSU (Xs) CCD observations. Phases were computed using a period of 18.703 days. The indicated zero-point shifts have been added to the U, R_C, and I_C curves to make the different light curves easier to see.

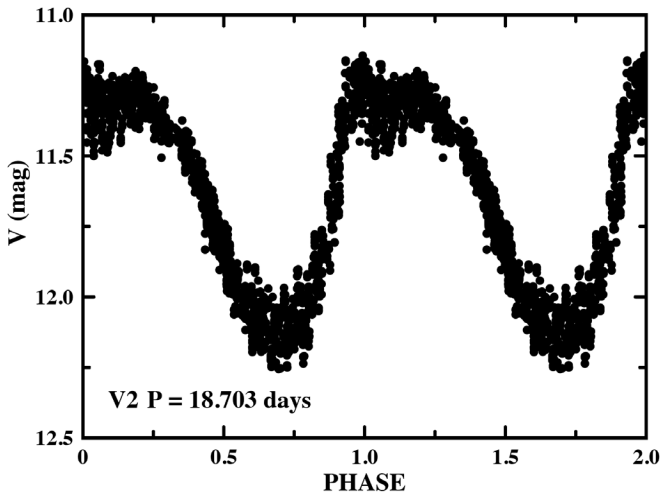

Figure 5. The light curve of all ASAS-SN V-band observations of V2, phased with a period of 18.703 days.

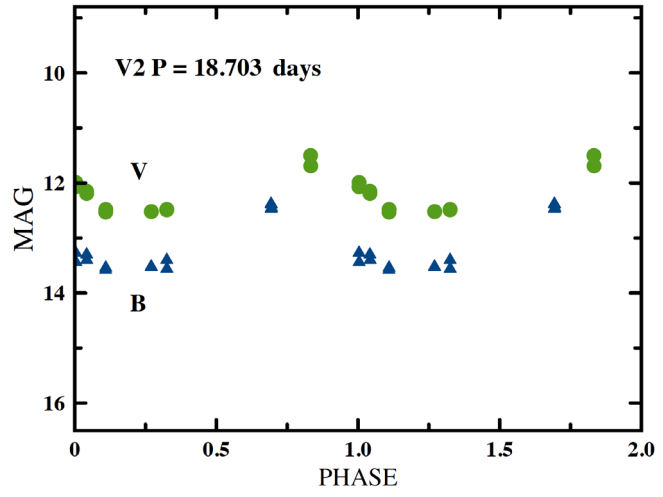

Figure 6. The B and V phased light curves of V2 from the photographic data. Phases were computed using a period of 18.703 days.

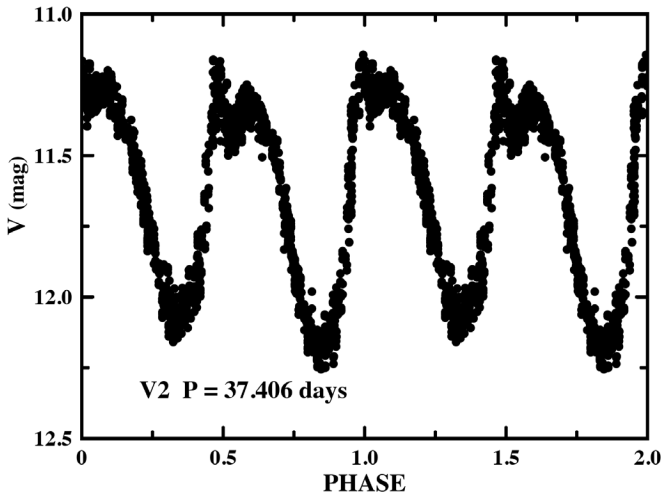

Figure 7. The light curve of all ASAS-SN V-band observations of V2, phased with a period of 37.406 days. Cycle differences, particularly the magnitude of minimum, are seen.

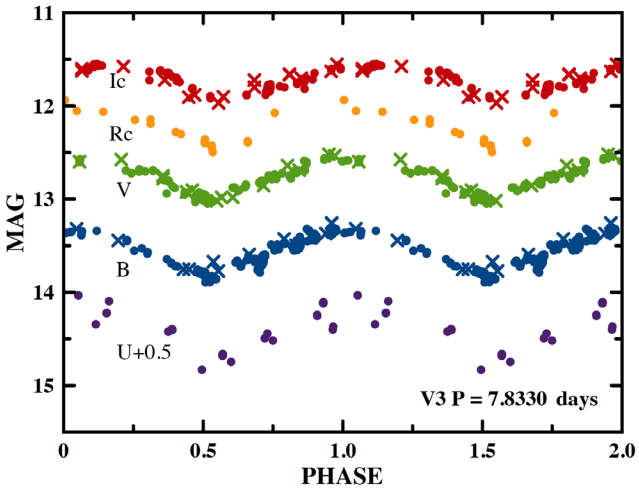

Figure 10. The U, B, V, R_C, and I_C-band phased light curves of V3 from the Stetson (dots) and MSU (Xs) observations. Phases were computed using a period of 7.8330 days. The indicated zero-point shift has been added to the U observations.

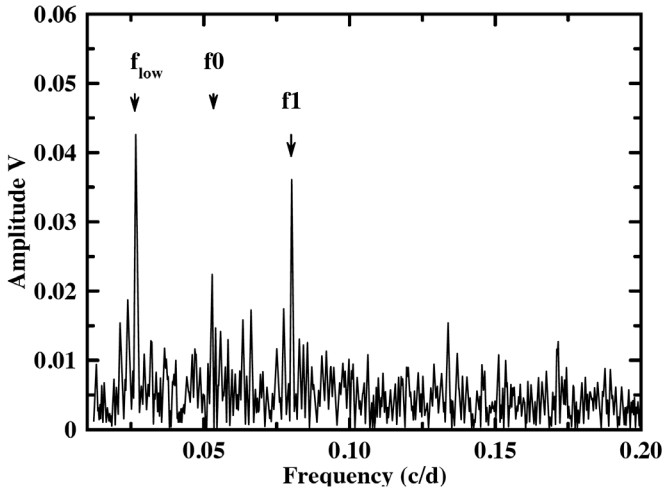

Figure 8. Fourier spectrum of the ASAS-SN V observations of V2 after removal of f_0 and its first five harmonics. Frequencies $f_{(low)}$ and f_1 are now dominant.

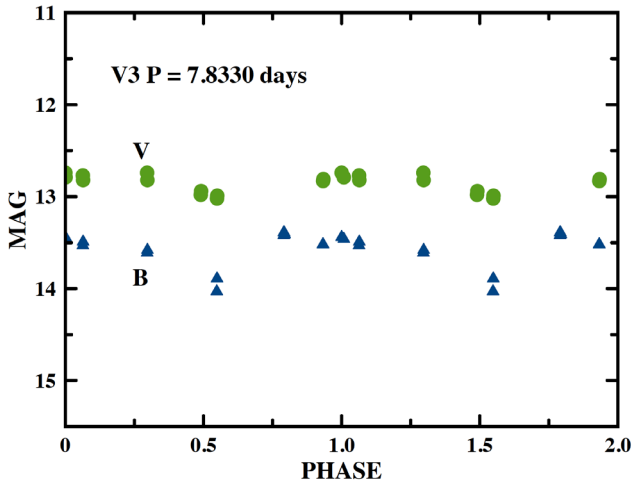

Figure 11. The B and V phased light curves of V3 from the photographic data. Phases were computed using a period of 7.8330 days.

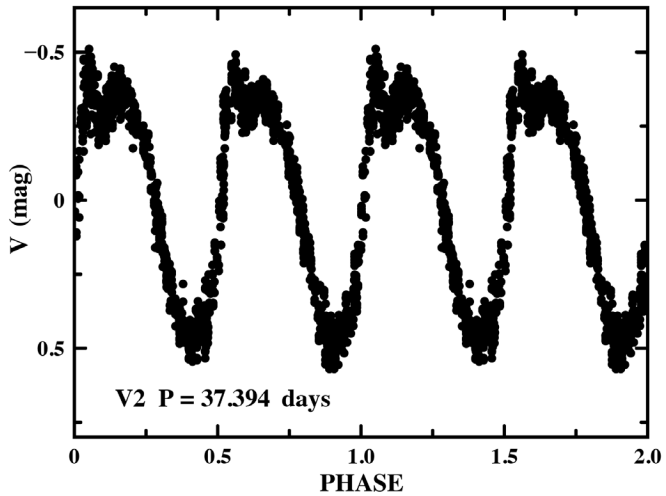

Figure 9. Subtracting frequencies $f_{(low)}$ and f_1 from the ASAS-SN data leaves a light curve with most of the alternate cycle variations seen in Figure 7 eliminated.

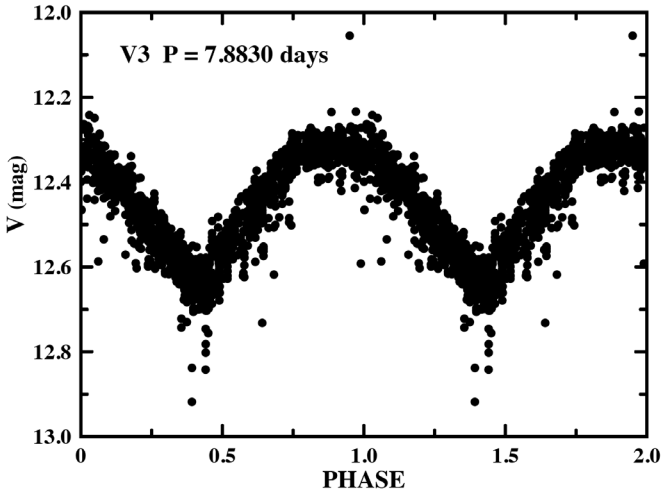

Figure 12. The light curve of all ASAS-SN V-band observations of V3, phased with a period of 7.8330 days.

Table 8. The magnitude-weighted mean magnitudes for V1, V2, and V3 using the Stetson and MSU photometry (and NURO for V1) and some results from the literature.

Star	*<U>*	*<B>*	*<V>*	*<R>*	*<I>*	*<B>–<V>*	*<V>–<I>*	*Source*
V1	14.59	13.40	11.94	11.00	10.32	1.46	1.62	Our results
V2	13.29	12.89	12.08	11.48	10.90	0.81	1.15	Our results
V3	13.88	13.57	12.78	12.29	11.73	0.79	1.05	Our results
V1	—	—	11.809	—	10.226	—	1.58	Arellano Ferro *et al.* (2020)
V2	—	—	12.127	—	10.934	—	1.19	Arellano Ferro *et al.* (2020)
V3	—	—	12.761	—	11.721	—	1.04	Arellano Ferro *et al.* (2020)
V1	—	—	11.83	—	—	1.52	—	Rozyczka *et al.* (2018), Table 1
V2	—	—	12.05	—	—	0.96	—	Rozyczka *et al.* (2018), Table 1
V3	—	—	12.75	—	—	0.87	—	Rozyczka *et al.* (2018), Table 1

Given the occurrence of period doubling, we used Period04 to perform a Fourier analysis for the extensive ASAS-SN V observations of V2. The results showed only one high-power frequency (denoted f_0), which corresponds to P = 18.697 d. We then performed a new search with f_0 and its harmonics ($2f_0$, $3f_0$, $4f_0$, $5f_0$, and $6f_0$) removed from the data. As shown in Figure 8, the new Fourier spectrum revealed two additional frequencies of significant power, which we name $f_{(low)}$ and f_1, following Templeton and Henden's (2007) similar analysis for W Vir. We then performed a simultaneous frequency search for f_0, f_1, and $f_{(low)}$, using the "improve all" option in Period04, while holding the harmonic terms fixed to f_0. Table 7 lists our final frequency and amplitude results. Values in parentheses indicate uncertainties returned by Period04. Amplitudes will, of course, be influenced by any blending effects from the large ASAS-SN pixels. The frequency f_0 found in this fashion corresponds to a period of 18.697 days, close to the V2 periods we found (see Table 6), and can be identified as the fundamental mode frequency (Bono *et al.* 2020).

The frequency pattern in Table 7 broadly matches that in Templeton and Henden's (2007) Table 2 for W Vir. They noted that, in the case of W Vir (main period 17.3 days), $f_{(low)}$ was similar but not identical, to both 0.5 f_0 and f_1–f_0. That is also the case for V2. Period doubling, that is alternating cycles having differences in light curve shape and amplitude, has now been identified for a number of W Vir stars, but especially those with periods longer than 15 days (Smolec *et al.* 2018; Jurkovic 2021). The presence of frequencies very near 0.5 f_0 and 1.5 f_0 in the Fourier spectrum of V2 is consistent with period doubling.

Given the 0.5 f_0 symmetry of $f_{(low)}$ and f_1 relative to f_0, it is tempting to say that W Vir alternate cycle effects result from a secondary period and its harmonics interacting with the fundamental mode of pulsation. In our case, that is supported by the fact that subtracting frequencies $f_{(low)}$ and f_1 from the ASAS-SN data leaves a light curve with most of the period doubling effects eliminated as shown in Figure 9, which can be compared to Figure 7.

Variable 3 Figure 10 shows the U, B, V, R_C, and I_C phased light curves of V3 from the Stetson and MSU CCD photometry using a period of 7.8330 days. Any variation of the time of maximum with wavelength is small. Figures 11 and 12 show, respectively, the light curves of V3 from the photographic observations and the ASAS-SN V data computed using the same period and epoch. The photographic curves agree with the CCD ones taking into account their larger errors. The ASAS-SN curve has similar phase but averages about 0.4 mag brighter than our V light curves, reflecting the blending effects seen in those observations.

Rozyczka *et al.* (2018) give a period of 7.872181 days for V3, somewhat higher than our value and the Clement *et al.* (1985) period of 7.831 days. The Arellano Ferro *et al.* (2020) period for V3, 7.835134 days, is closer to our own, although still a little higher.

4. Mean magnitudes

We have determined mean magnitudes for V1, V2, and V3 from our observations. These are given in Table 8 with some results from previous studies for comparison. Our means are magnitude averages over phase for V2 and V3. That, however, was not possible for the red semiregular variable V1, so those values are averages over time from the Stetson and MSU observations. Mean magnitudes from the ASAS-SN photometry are not listed in Table 8 because that camera's large pixels make images subject to blending. No corrections for interstellar extinction have been applied to the mean magnitudes, although we note that Arellano Ferro *et al.* (2020) adopted E(B–V) = 0.25 for the cluster.

5. Long term period changes

Clement *et al.* (1985) investigated the long-term period changes of V2 and V3 using the photographic observations then available. Their Table II and Figure 4 show the relative phase shifts of the light curves of V2 and V3 at different epochs, determined using their adopted periods of 18.7226 days and 7.831 days for V2 and V3. We double-checked the Clement *et al.* (1985) phase shift values to verify that we find the same shifts to within the expected uncertainties. One exception was the phase shift for the 1932 observations of V3, for which we find a shift of 0.01 preferable to the Clement *et al.* value of 0.11. Our estimated error for that point is, however, large, about 0.1.

We used our more recent data to extend the time coverage of the period change investigations. The B and V light curves from photometry in our datasets (1) through (5) were used to determine relative phase shifts for recent epochs on the Clement *et al.* (1985) system. We did not use our U, R_C, and I_C-band

Table 9. Phase shifts of maximum light of V2 (in fractions of a period).

Year	*Shift*	*Error*	*Source*
1912–1919	0.05	0.12	Clement *et al.* (1985), Table II
1931–1934	–0.17	0.04	Clement *et al.* (1985), Table II
1935–1936	–0.16	0.07	Clement *et al.* (1985), Table II
1937–1939	–0.13	0.06	Clement *et al.* (1985), Table II
1940–1949	–0.04	0.08	Clement *et al.* (1985), Table II
1948–1949	0.02	0.06	Clement *et al.* (1985), Table II
1950–1957	–0.02	0.06	Clement *et al.* (1985), Table II
1951–1952	0.02	0.10	Clement *et al.* (1985), Table II
1952	0.00	0.02	Clement *et al.* (1985), Table II
1954	0.01	0.04	Clement *et al.* (1985), Table II
1954–1956	0.01	0.08	Clement *et al.* (1985), Table II
1957	0.02	0.07	Clement *et al.* (1985), Table II
1959–1968	0.01	0.05	Clement *et al.* (1985), Table II
1968–1971	0.05	0.09	Clement *et al.* (1985), Table II
1972	0.04	0.07	Clement *et al.* (1985), Table II
1972–1973	0.04	0.05	Clement *et al.* (1985), Table II
1973–1974	0.02	0.05	Clement *et al.* (1985), Table II
1975	0.04	0.10	Clement *et al.* (1985), Table II
1979	0.01	0.05	Clement *et al.* (1985), Table II
1980–1983	0.10	0.10	Clement *et al.* (1985), Table II
1983	–0.12	0.12	USNO plates
1996–2000	–0.26	0.12	Stetson
2001–2011	–0.29	0.08	Stetson, MSU
2012	–0.55	0.12	ASAS-SN
2013	–0.60	0.05	ASAS-SN
2012–2018	–0.42	0.12	Stetson
2014	–0.62	0.03	ASAS-SN
2015	–0.66	0.03	ASAS-SN
2016	–0.66	0.03	ASAS-SN
2017	–0.68	0.03	ASAS-SN
2018	–0.68	0.03	ASAS-SN
2019	–0.69	0.03	ASAS-SN
2020	–0.72	0.03	ASAS-SN

Table 10. Phase shifts of maximum light of V3 (in fractions of a period).

Year	*Shift*	*Error*	*Source*
1932	0.01	0.10	Clement *et al.* (1985) (modified)
1933	–0.22	0.08	Clement *et al.* (1985), Table II
1935–1936	–0.22	0.15	Clement *et al.* (1985), Table II
1937	–0.25	0.06	Clement *et al.* (1985), Table II
1938–1940	–0.09	0.10	Clement *et al.* (1985), Table II
1941–1949	–0.17	0.15	Clement *et al.* (1985), Table II
1948–1952	–0.02	0.07	Clement *et al.* (1985), Table II
1952	0.00	0.01	Clement *et al.* (1985), Table II
1954	–0.10	0.05	Clement *et al.* (1985), Table II
1954	0.14	0.06	Clement *et al.* (1985), Table II
1955	0.05	0.08	Clement *et al.* (1985), Table II
1957	0.11	0.10	Clement *et al.* (1985), Table II
1956–1960	0.03	0.22	Clement *et al.* (1985), Table II
1961–1968	0.08	0.10	Clement *et al.* (1985), Table II
1968–1972	–0.05	0.08	Clement *et al.* (1985), Table II
1972–1973	–0.02	0.08	Clement *et al.* (1985), Table II
1973–1975	0.01	0.06	Clement *et al.* (1985), Table II
1979	–0.02	0.07	Clement *et al.* (1985), Table II
1980	0.03	0.07	Clement *et al.* (1985), Table II
1983	0.04	0.08	USNO plates
1992	–0.04	0.15	Las Campanas plates
1996–2000	0.07	0.08	Stetson
2006	0.18	0.09	MSU
2001–2011	0.11	0.05	Stetson
2012	0.20	0.12	ASAS-SN
2013	0.24	0.04	ASAS-SN
2012–2018	0.23	0.05	Stetson
2014	0.25	0.03	ASAS-SN
2015	0.26	0.03	ASAS-SN
2016	0.27	0.03	ASAS-SN
2017	0.28	0.03	ASAS-SN
2018	0.29	0.03	ASAS-SN
2019	0.30	0.03	ASAS-SN
2020	0.31	0.03	ASAS-SN

light curves for phase shift determinations as they differ too greatly in shape compared to the V and B band light curves. Allowance was made for a small difference between the B and V light curves of V2 in that its V light curve is shifted to longer phases by 0.03 ± 0.02 relative to B. For the ASAS-SN observations, light curves were determined for each year for which a sufficient number of observations was available. Because of the long time coverage of the Stetson CCD data, those observations were divided into three separately-treated sets: 1996–2000, 2001–2011, and 2012–2018.

Following Clement *et al.* (1985), we adopted the Arp (1955) observations from 1952 as having a phase shift of 0.00 and used the Clement *et al.* periods of 18.7226 days for V2 and 7.831 days for V3 for computing our light curves. Our curves were then compared to light curves from several datasets in Table II of Clement *et al.* (1985) and the relative phase shifts determined for each case. When both B and V light curves were available for an epoch, the shift results were averaged to obtain the adopted value. We emphasize that for many of the datasets in Table II of Clement *et al.* (1985), as well as for our more sparse new datasets, using the entire light curve to determine a phase shift is preferable to determining an O–C value using just the data near maximum or near minimum light.

Our adopted phase shifts for V2 and V3 are listed in Tables 9 and 10, respectively. The listed errors are those given by Clement *et al.* (1985) for their data, while for ours they are eye estimates of how uncertain the phase shift determination was when comparing our light curve to the Clement *et al.* reference ones. The time of maximum of V3 from Table 3 in Arellano Ferro *et al.* (2020) has been neglected because it was calculated using a period different from ours and the ASAS-SN observations already provide good recent time coverage around their epoch.

The phase shifts are shown as a function of time in Figures 13 and 14. The cycle count for the point representing the 1912–1919 observations of V2 is uncertain. The point could be plotted at a phase shift of 0.05 or –0.95. Inspection of Figure 13 reveals a decreasing period for V2. Figure 14 shows a nearly constant period for V3, although some fluctuation in period is possible. The slope of the phase shift–date correlation reflects a slight difference between the period adopted by Clement *et al.* (1985) and the average period over the 90 years covered by our data.

Period change rates for RR Lyrae stars and Cepheids are often described as the rate of period change in days per million years, denoted by β (see, for example, Le Borgne *et al.* 2007, Equation 3, and Osborn *et al.* 2019, Equation 5). In calculating β for V2, we excluded the 1912–1919 point because of its cycle count ambiguity. A parabolic least squares fit to the other phase shift points in that table, weighted by $1/\text{error}^2$, yielded $\beta = -452 \pm 23$ d/Myr, thus confirming a significantly decreasing period.

The –0.95 phase shift option for the 1912–1919 observations for V2 is most consistent with our decreasing period result.

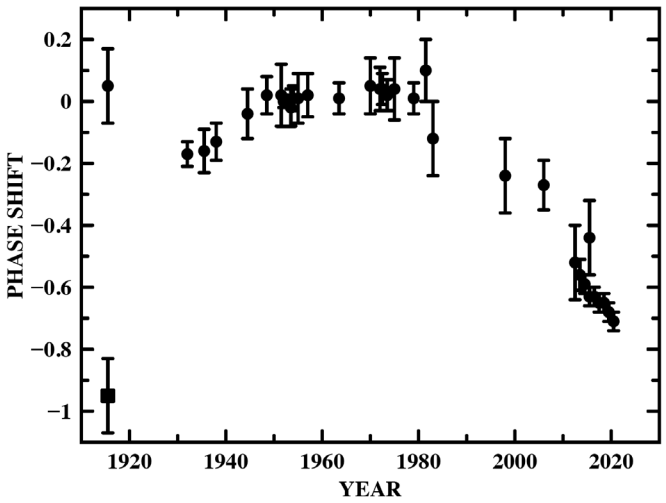

Figure 13. The phase shift diagram for V2. Two alternative shifts are possible for the first data point because of a cycle count ambiguity. The data indicate a significant period decrease.

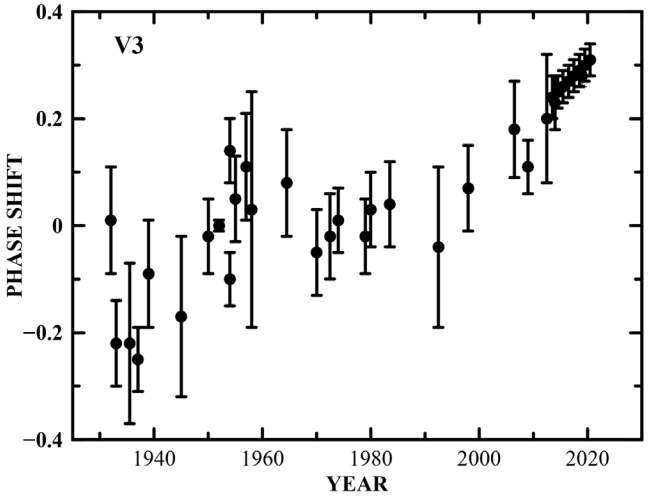

Figure 14. The phase shift diagram for V3. No obvious evidence of a period change is seen.

For V3, we calculated $\beta = +7.9 \pm 7.8$ d/Myr, indicating any long-term period increase is doubtful. The overall slope of the points is consistent with an average period of 7.832 days.

6. Conclusions

Our observations confirm that V1 is a red semiregular variable. We find a B–V of 1.46 and that the light variations cycle on a time scale of about 49 days, at least over the past few decades.

V2 and V3 are type II Cepheids. These are commonly divided into two subtypes, the BL Her stars, with $P \leq 5$ d, and the longer period W Vir ones, having $5 \text{ d} < P \leq 20$ d, while the related stars with periods longer than 20 d are called RV Tau variables (Soszyński *et al.* 2011; Bono *et al.* 2020). Thus, both stars are W Vir subtype.

The period of V2, P = 18.70 d, falls near the upper end of the range of W Vir periods, close to the period range for RV Tau stars. Period doubling, such as seen in V2, is often exhibited by RV Tau variables. On the other hand, the period of V3, P = 7.8330 d, is near the lower end of the W Vir period range.

W Virginis variables have been observed to have increasing periods, decreasing periods, or even erratic period changes (Neilson *et al.* 2016; Karmakar *et al.* 2019). The decreasing period of V2 is thus not extraordinary. As noted in Neilson *et al.* (2016), however, interpreting the observed period changes of W Vir stars is made difficult by uncertainties concerning the mechanism by which such stars enter the instability strip. Bono *et al.* (2020) predicted that W Vir variables should show both period increases and decreases, but that increases should be more commonly observed. Negative period changes should mainly affect the long-period tail of the W Vir stars in their model, which would apply to V2. However, Bono *et al.* (2020) also noted that those conclusions might need to be altered if gravo-nuclear loops occur inside the instability strip, something not included in their model.

Relatively few type II Cepheids are found with periods of 5 to 8 days in galactic globular clusters, although that period range is more populated in some other systems (see Figure 4 in Soszyński *et al.* 2011 and Figure 2 in Bono *et al.* 2020). While the period of V3 makes it by definition too long for inclusion in the BL Her class, it might be considered as in the transition range between W Vir and BL Her subtypes. Metal-poor BL Her variables with measured rates of period change have increasing or constant periods (see Wehlau and Bohlender 1982 and Osborn *et al.* 2019, Table 9). The nearly constant period of V3 is consistent with the behavior of BL Her variables. Further, some BL Her stars have been observed to exhibit short term period fluctuations (Osborn *et al.* 2019), as our O–C results suggest may be the case for V3.

7. Acknowledgements

We thank Christine Clement for her help and advice and Yerkes Observatory for allowing access to its photographic plate archive. This research made use of the Peranso light curve and period analysis software. We thank the ASAS-SN project for providing public access to its observations. We thank those who created and who maintain the Period04 program. We thank the anonymous referee for the detailed comments that allowed us to significantly improve the paper.

References

Arellano Ferro, A., Yepez, M. A., Muneer, S., Bustos Fierro, I. H., Schröder, K. P., Giridhar, S., and Calderón, J. H. 2020, *Mon. Not. Roy. Astron. Soc.*, **499**, 4026.

Arp, H. C. 1955, *Astron. J.*, **60**, 1.

Bono, G., *et al.* 2020, *Astron. Astrophys.*, **644**, A96.

Clement, C. M., Hogg, H. S., and Wells, T. R. 1985, *Astron. J.*, **90**, 1238.

Clement, C. M., *et al.* 2001. *Astron. J.*, **122**, 2587.

Jurkovic, M. I. 2021, in *RR Lyrae/Cepheid 2019: Frontiers of Classical Pulsators*, ASP Conf. Ser. 529, eds. K. Kinemuchi, C. Lovekin, H. Neilson, K. Vivas, Astronomical Society of the Pacific, San Francisco, 305.

Karmakar, P., Smith, H. A., and De Lee, N. 2019, *J. Amer. Assoc. Var. Star Obs.*, **47**, 167.
Kochanek, C. S., *et al.* 2017, *Publ. Astron. Soc. Pacific*, **129**, 104502 (https://asas-sn.osu.edu).
Le Borgne, J. F., *et al.* 2007, *Astron. Astrophys.*, **476**, 307.
Lenz P., and Breger M. 2005, *Commun. Asteroseismology*, **146**, 53.
Neilson, H. R., Percy, J. R., and Smith, H. A. 2016, *J. Amer. Assoc. Var. Star Obs.*, **44**, 179.
Osborn, W., Kopacki, G., Smith, H. A., Layden, A., Pritzl, B., Kuehn, C., and Anderson, M. 2019, *Acta Astron.*, **69**, 101.
Paunzen, E., and Vanmunster, T. 2016, *Astron. Nachr.*, **337**, 239.
Plachy, E., Molnár, L., Jurkovic, M. I., Smolec, R., Moskalik, P. A., Pál, A., Szabados, L., and Szabó, R. 2017, *Mon. Not. Roy. Astron. Soc.*, **465**, 173.
Rabidoux, K., *et al.* 2010, *Astron. J.*, **139**, 2300.
Rozyczka, M., Narloch, W., Schwarzenberg-Czerny, A., Thompson, I. B., Poleski, R., and Pych, W. 2018, *Acta Astron.*, **68**, 237.
Samus, N. N., Kazarovets, E. V., Durlevich, O. V., Kireeva, N. N., and Pastukhova, E. N. 2017, *Astron. Rep.*, **61**, 80, *General Catalogue of Variable Stars: Version GCVS 5.1* (http://www.sai.msu.su/gcvs/gcvs/index.htm).
Shappee, B. J., *et al.* 2014, *Astrophys. J.*, **788**, 48 (https://asas-sn.osu.edu).
Smolec, R., and Moskalik, P. 2012, *Mon. Not. Roy. Astron. Soc.*, **426**, 108.
Smolec, R., Moskalik, P., Plachy, E., Soszyński, I., and Udalski, A. 2018, *Mon. Not. Roy. Astron. Soc.*, **481**, 3724.
Soszyński, I., *et al.* 2011, *Acta Astron.*, **61**, 285.
Stetson, P. B. 1987, *Publ. Astron. Soc. Pacific*, **99**, 191.
Stetson, P. B. 1994, in *Astronomy with the CFHT Adaptive Optics Bonnette*, ed. R. Arsenault, Canada-France-Hawaii Telescope Corp., Kamuela, HI, 72.
Stetson, P. B., Pancino, E., Zocchi, A., Sanna, N., and Monelli, M. 2019, *Mon. Not. Roy. Astron. Soc.*, **485**, 3042.
Templeton, M. R., and Henden, A. A. 2007, *Astron. J.*, **134**, 1999.
Vanmunster, T. 2006, Peranso 2.0 Manual, CBA Belgium (https://www.cbabelgium.com/peranso).
Wehlau, A., and Bohlender, D. 1982, *Astron. J.*, **87**, 780.